Hindawi Publishing Corporation
International Journal of Aerospace Engineering
Volume 2015, Article ID 769862, 14 pages
http://dx.doi.org/10.1155/2015/769862

Research Article

Ligament and Droplet Generation by Oil Film on a Rotating Disk

Hengchao Sun, Guoding Chen, Li'na Wang, and Fei Wang

School of Mechanical Engineering, Northwestern Polytechnical University, Xi'an 710072, China

Correspondence should be addressed to Guoding Chen; gdchen@nwpu.edu.cn

Received 10 July 2015; Revised 17 September 2015; Accepted 21 September 2015

Academic Editor: Saad A. Ahmed

The lubrication and heat transfer designs of bearing chamber depend on an understanding of oil/air two-phase flow. As initial and boundary conditions, the characteristics of ligament and droplet generation by oil film on rotating parts have significant influence on the feasibility of oil/air two-phase flow analysis. An integrated model to predict the oil film flow, ligament number, and droplet Sauter mean diameter (SMD) of a rotating disk, which is an abstraction of the droplet generation sources in a bearing chamber, is developed based on the oil film force balance analysis and wave theory. The oil film thickness and velocity, ligaments number, and droplet SMD are calculated as functions of the rotating disk radius, rotational speed and oil volume flow rate and oil properties. The theoretical results show that the oil film thickness and SMD are decreased with an increasing rotational speed, while the radial, transverse velocities, and ligament number are increased. The oil film thickness, radial velocity, and SMD are increased with an increasing oil flow rate, but the transverse velocity and ligament number are decreased. A test facility is built for the investigation into the ligament number of a rotating disk, and the measurement of ligament number is carried out by means of a high speed photography.

1. Introduction

Bearing chamber is an important component of aeroengine and it gives a guarantee of shaft running reliably. To address the demands of modern aero engines development tendency, for example, higher compressor pressure ratio, operating temperature, and shaft speed, the need to promote the performance of bearing chamber becomes more obvious, while the sufficient lubrication and cooling designs of bearing chamber relate to the understanding of oil/air two-phase flow which includes air, oil droplets, and oil film. Therefore, special efforts have been made to carry out the research on that in recent years.

Several researchers have conducted the theoretical and experimental investigations onto the oil/air two-phase flow in bearing chamber. Their works focused on the characteristic of oil droplets which are atomized by rotating parts [1–7], oil droplet motion, and deposition on chamber housing [8–10], as well as oil film flow with chamber housing [11–14]. Among the oil/air two-phase flow in bearing chamber, the droplet is given more attention. The reasons are that the droplet affects the safety and reliability of bearing chamber. Smaller droplets may lead to more oil consumption when the droplets pass via the vent of bearing chamber. In addition, the appearance of smaller droplets is a potential risk of oil fire inside bearing chamber. The oil droplet characteristics, such as oil droplet size distribution and velocity, are initial and boundary conditions for the oil droplet motion and subsequent analysis.

In the scope of oil droplet characteristics in bearing chamber, some experimental works have been carried out. Wittig et al. [15] developed and built a test facility which allowed for the first time a detailed investigation into oil/air flow phenomena and related heat transfer processes in bearing chamber. On the test facility, Glahn et al. [1] carried out experimental investigation on size and velocity of droplet which was atomized by bearing. Gorse et al. [2] recorded the phenomenon of oil droplets which were generated near the bearing by double-shutter-CCD cameras. And it was observed that the design of bearing support has strong influence on the generation of droplet. Shimo et al. [3] dealt with the oil which sprayed onto a seal runner and discussed the oil velocity and thickness

on the seal runner based on thin-film theory. Krug et al. [4] gained an insight into the interaction of oil jet with underrace lubrication collector. It was observed that the oil droplets were shed at the edge of collector outer. Glahn et al. [5] found that the droplet generation process in the bearing chamber was similar to the liquid atomization process in a rotary atomizer; therefore, a rotating disk chamber test rig was built [6, 7]. The documentation of oil droplets generation around the rotating disk was obtained. It was found that the oil film on the rotating disk disintegrated into a lot of ligaments and droplets [5]; in addition, the droplet diameter and velocity were measured by the PDPA. The abstraction of droplet generation sources in bearing chamber which was proposed by Glahn et al. promotes the measuring accuracy due to the simple structure and better accessibility of the optical device. Their work develops a new approach for the investigation into the oil droplet characteristics in a bearing chamber.

However, little theoretical work about the oil droplet which is atomized by rotating parts in the bearing chamber could be found, and the experiments which are suitable for various conditions are extremely time and finance consuming. Therefore, it is necessary to investigate the droplet generation characteristics in the bearing chamber. In this paper, firstly, a rotating disk structure which is an abstraction of droplet generation sources in the bearing chamber is determined. And then the centrifugal force which exerts on the oil film flowing on a rotating disk is proposed. With the force balance and Newton fluid behavior, the oil film thickness and velocity are calculated. Secondly, when the oil film reaches the rotating disk edge, the oil film wave characteristic is discussed and the gas pressure, surface tension force, inertia force, and viscous shear force which act on the wavy film are determined. With that the equation which involves wave growth rate is derived. The wave growth rate can evaluate the oil film disintegration. Solving the equation, the ligament number and oil droplet Sauter mean diameter (SMD) are obtained lastly. A test facility for the investigation into the droplet generation characteristics of a rotating disk is built. The measurement of ligament number is carried out by means of a high speed photography. The comparison of theoretical and experimental results supports the reliability of the proposed method. The work may be helpful to improve the research system of oil/air two-phase flow in the bearing chamber.

2. An Abstraction of the Droplet Generation Sources in a Bearing Chamber

The droplet generation process in an aeroengine bearing chamber is shown in Figure 1. For the purpose of lubrication and cooling, the oil which is supplied by some nozzles is injected into the gap between the collector and shaft, and then the oil is fed on the bearing via underrace lubrication. In addition, the oil also impacts the rotor of seal. For underrace lubrication, only a certain amount of the supplied oil is fed to bearing, and the oil film which spreads on the bearing elements is atomized to a lot of droplets when the oil passes the bearing. The rest which is not caught by the collector is distributed by the surrounding air and also changes to a lot of oil

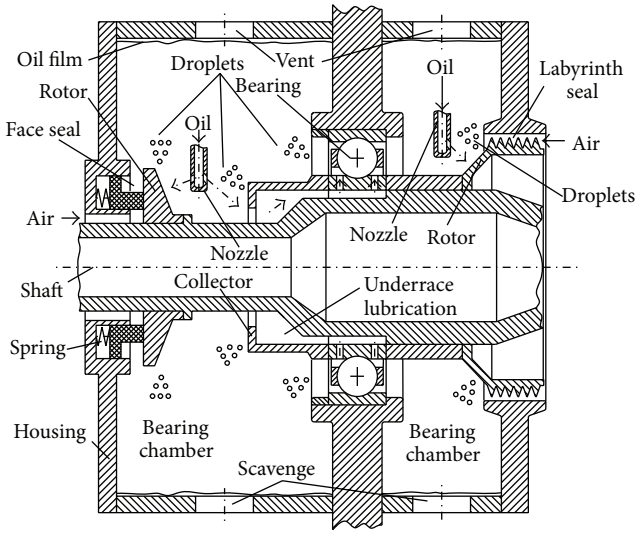

Figure 1: Droplet generation and oil/air two-phase flow in a bearing chamber.

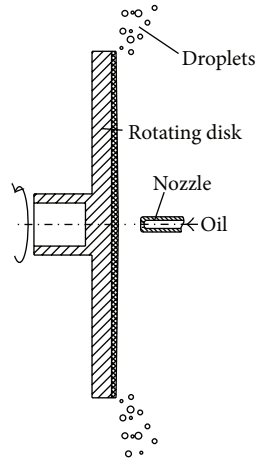

Figure 2: An abstraction of the droplet generation sources in a bearing chamber.

droplets lastly. Similarly, the oil which impacts the seal rotor will spread on its surface and be disintegrated to oil droplets. The chamber is sealed by buffer air, and, due to the angular momentum which is transferred from the rotating parts, the oil droplets are ejected into the rotating airflow and move to chamber housing. Furthermore, the droplets impinge on the chamber housing and an oil film appears. Ultimately, a complex oil/air two-phase flow occurs in the bearing chamber.

As mentioned in [5–7], the basic flow features of the droplet generation process in bearing chamber show remarkable similarities to the flow in rotary atomizers [16–19]. That is, as shown in Figure 2, the liquid is fed onto a rotating surface, for example, a flat disk, where the liquid spreads out under the action of centrifugal force. When flowing around the edge of rotating disk, the oil film will be disintegrated and that results in the formation of some cylindrical liquid ligaments. The ligament will eventually form a satellite

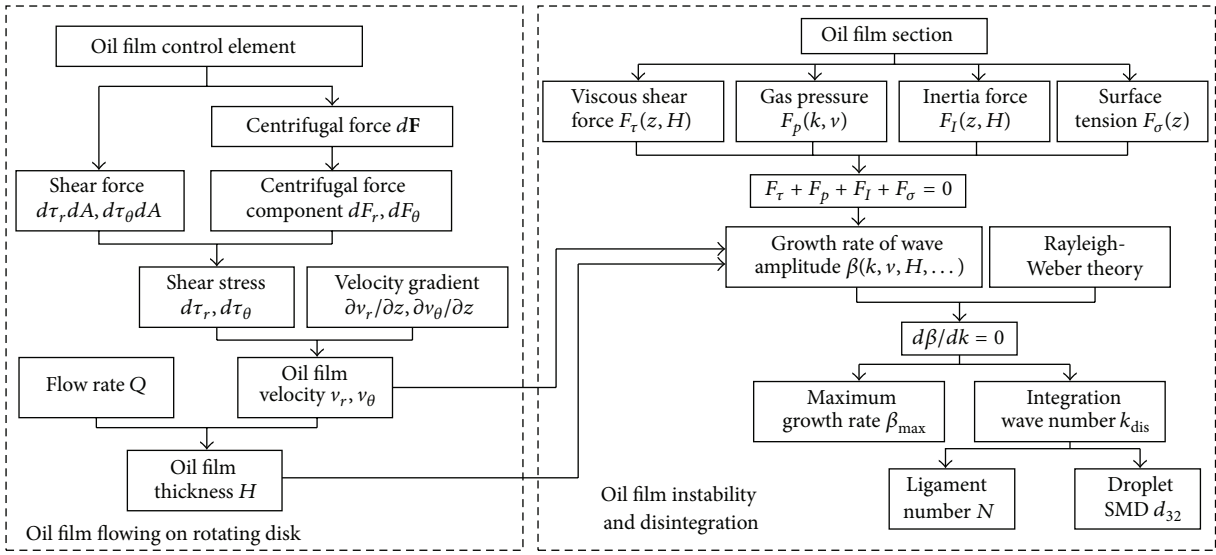

Figure 3: Calculation scheme for the theoretical model.

droplet or if the ligament is long enough, it may further break up into even smaller droplets [5]. For the sake of convenience, the extremely complicated and detailed design which is found in actual engine bearing chamber is omitted in the present paper and the flow regime of oil on underrace lubrication collector, bearing, and seal rotor is treated as the oil flowing on a rotating flat disk based on a reasonable simplification. In addition, the geometry and operating parameters are determined according to the bearing chamber.

3. Theoretical Model Development

A simplified structure for investigation into the droplet generation characteristics in the bearing chamber is determined in Section 2, namely, the rotating disk. The oil film flowing on the disk, oil film disintegration, ligament number, and oil droplet SMD are analyzed step by step in this section. Figure 3 summarizes the determination process of the oil film thickness, velocity, ligament number, and droplet SMD.

3.1. Oil Film Velocity and Thickness on a Rotating Disk

3.1.1. Coordinate System and Control Element. In Figure 4, a cylindrical-coordinate system r-θ-z is fixed on the rotating disk; in addition, the z coordinate axis coincides with the rotation axis of rotating disk. The rotating disk angular velocity is ω. A small control element is divided from the oil film which is flowing on the rotating disk at any position (r, θ, and z). The control element volume and sizes in axial, radial, and transverse directions are dV, dz, dr, and $d\theta$ respectively. The areas of the two sides which are perpendicular to the z direction are dA; obviously, $dA = dV/dz$.

3.1.2. Assumptions. Prior to the proposition of oil film velocity and thickness analysis model, some reasonable assumptions have been made as follows. (1) The oil film flowing on the rotating disk is continuous, and its velocity and thickness distributions are axisymmetric (i.e., not vary in transverse direction). (2) Due to the extremely thin thickness, the pressure in film is considered constant and equal to that in environment. (3) Compared to the centrifugal force, the gravitational force is neglected. (4) The other inertial forces are omitted except for centrifugal force. (5) The oil is a Newtonian fluid with a constant viscosity and incompressible, (6) The oil has no relative movement at the interface between oil film and rotating disk.

3.1.3. Centrifugal Force on the Control Element. Because of the coordinate system r-θ-z rotating together with the rotating disk, the motion and force analysis of the oil film is carried out under a noninertial reference frame. According to the D'Alembert principle, the Coriolis acceleration and centripetal acceleration should be considered. Thus, the centrifugal force $d\mathbf{F}$, which exerts on the oil film control element, is given by [20]

$$d\mathbf{F} = -\rho \left[2\boldsymbol{\omega} \times \mathbf{v} + \boldsymbol{\omega} \times (\boldsymbol{\omega} \times \mathbf{r})\right] dV, \tag{1}$$

where ρ is the oil density, $\boldsymbol{\omega}$ is the angular velocity vector of the rotating disk, $\mathbf{v}$ is the control element velocity vector relative to the rotating disk, $\mathbf{r}$ is the control element radial coordinate vector, $2\boldsymbol{\omega} \times \mathbf{v}$ is the Coriolis acceleration, and $\boldsymbol{\omega} \times (\boldsymbol{\omega} \times \mathbf{r})$ is the centripetal acceleration.

The components of the centrifugal force $d\mathbf{F}$ in transverse and radial directions are expressed in terms of $d\mathbf{F}_\theta$ and $d\mathbf{F}_r$, respectively. The unit vectors in r, θ, and z directions are defined as $\mathbf{e}_r$, $\mathbf{e}_\theta$, and $\mathbf{e}_z$, respectively. The centrifugal force $d\mathbf{F}$, angular velocity vector $\boldsymbol{\omega}$, velocity vector $\mathbf{v}$, and radial coordinate vector $\mathbf{r}$ are rewrote by their components

$$d\mathbf{F} = dF_r \mathbf{e}_r + dF_\theta \mathbf{e}_\theta + dF_z \mathbf{e}_z, \tag{2a}$$

$$\boldsymbol{\omega} = \omega \mathbf{e}_z, \tag{2b}$$

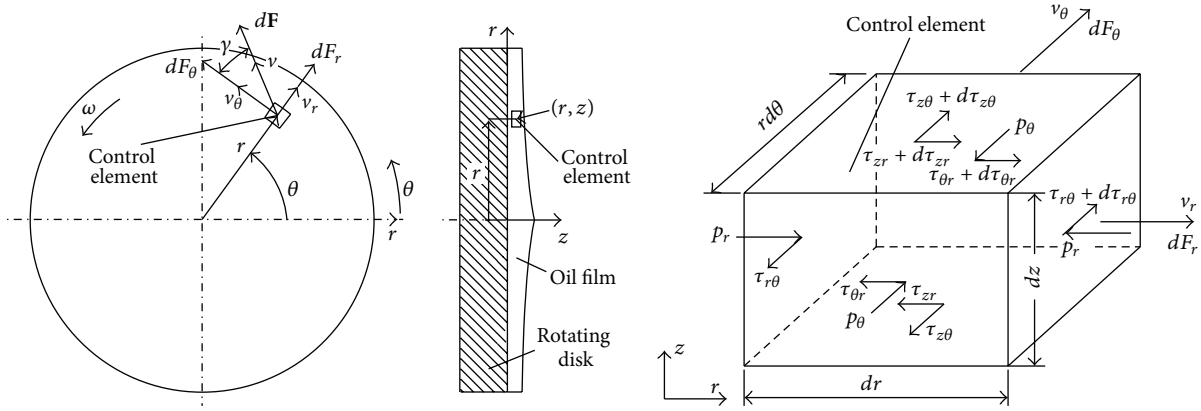

(a) Oil film control element

(b) Forces on the control element

Figure 4: Oil film control element and forces on its surfaces.

$$\mathbf{v} = v_r\mathbf{e}_r + v_\theta\mathbf{e}_\theta + v_z\mathbf{e}_z = v_r\mathbf{e}_r + v_\theta\mathbf{e}_\theta, \tag{2c}$$

$$\mathbf{r} = r\mathbf{e}_r. \tag{2d}$$

Substituting (2a), (2b), (2c), and (2d) into (1), we can obtain the centrifugal force $d\mathbf{F}$

$$d\mathbf{F} = -\rho dV\left[\left(-2\omega v_\theta - \omega^2 r\right)\mathbf{e}_r + 2\omega v_r\mathbf{e}_\theta\right]. \tag{3}$$

3.1.4. Oil Film Velocity and Thickness in Radial Direction. The radial component of centrifugal force $d\mathbf{F}$, which exerts on the oil film control element $d\mathbf{F}_r = \rho(2\omega v_\theta + \omega^2 r)dV\mathbf{e}_r$, is shown in (4). The extremely thin oil film does not slip very much on the rotating disk; namely, the relative velocity of oil film to rotating disk v_θ is much less than the linear velocity of rotating disk ωr. As a result, the term of $2\omega v_\theta$ could be neglected compared to $\omega^2 r$. Therefore, $d\mathbf{F}_r$ is given by

$$dF_r \approx \rho_l\omega^2 r dV. \tag{4}$$

As shown in Figure 4, according to assumption (2), the pressure forces p_r on the control element two sides which are perpendicular to r direction canceled each other out. According to assumption (1), the radial velocity gradient in transverse direction on the control element two sides which are perpendicular to θ direction is zero; in other words, $(\partial v_r/\partial\theta)/r = 0$. Therefore, the shear stresses in radial direction on the above two sides are that $\tau_{\theta r} = \mu(\partial v_r/\partial\theta)/r \mid \Gamma_F = 0$ and $\tau_{\theta r} + d\tau_{\theta r} = \mu(\partial v_r/\partial\theta)/r \mid \Gamma_B = 0$. It is defined that the force positive direction is along the positive direction of r coordinate. As mentioned above, the resultant force acting on the control element in radial direction is the composition of only the radial centrifugal force dF_r and the radial viscous shear forces $\tau_{zr}dA$ and $(\tau_{zr}+d\tau_{zr})dA$. Lastly, with assumption (4), the resultant force in the radial direction is zero:

$$\left(\tau_{zr} + d\tau_{zr}\right)dA - \tau_{zr}dA + dF_r = 0. \tag{5}$$

Using (4) and (5), the elemental radial viscous shear stress $d\tau_{zr}$ can be solved simultaneously

$$d\tau_{zr} = \frac{dF_r}{dA} \approx -\rho\omega^2 r\, dz, \tag{6}$$

or

$$\frac{d\tau_{zr}}{z} = -\rho\omega^2 r. \tag{7}$$

Equation (7) can be integrated to give

$$\tau_{zr} = -\rho\omega^2 rz + C_1. \tag{8}$$

The integration constant C_1 could be determined with the boundary condition. For the free surface of oil film that is the interface between oil film and air (the axial coordinate z equals to the oil film thickness H), the viscous shear stress $\tau_{zr} = 0$. Thus, the integration constant $C_1 = \rho\omega^2 rH$. And then, at any internal position of the oil film, where the axial distance from the rotating disk is z, the radial viscous shear stress is given by

$$\tau_{zr} = \rho\omega^2 r\left(H - z\right). \tag{9}$$

For a Newtonian fluid, the relation between viscous shear stress and velocity gradient is generally known as

$$\tau_{zr} = \mu\frac{\partial v_r}{\partial z}. \tag{10}$$

Using (9) and (10), we can obtain

$$\frac{\partial v_r}{\partial z} = \frac{\rho\omega^2 r}{\mu}\left(H - z\right). \tag{11}$$

Equation (11) can be integrated to give

$$v_r = \frac{\rho\omega^2 r}{\mu}\left(Hz - \frac{z^2}{2} + C_2\right). \tag{12}$$

The integration constant C_2 could be also determined with the boundary condition. At the interface between oil film and rotating disk ($z = 0$), the relative velocity between oil film and rotating disk $v_r = 0$. Therefore, the integration constant $C_2 = 0$. And then, the oil film radial velocity at any axial position z $(0 \le z \le H)$ is

$$v_r = \frac{\rho\omega^2 r}{\mu}\left(Hz - \frac{z^2}{2}\right). \tag{13}$$

For a steady and incompressible flow, the total volume flow rate of the oil film at radial position r is

$$\int_0^{2\pi}\int_0^H v_r r\,dz\,d\theta = Q, \tag{14}$$

where Q denotes the volume flow rate of oil which is supplied to the rotating disk.

Substituting (13) into (14), the oil film thickness H and average radial velocity at radial position r could be determined, respectively, as follows:

$$H = \left[\frac{3\mu Q}{2\pi\rho\omega^2 r^2}\right]^{1/3}, \tag{15}$$

$$\overline{v_r} = \frac{Q}{2\pi rH} = \frac{1}{2}\left[\frac{2\rho\omega^2 Q^2}{3\pi^2\mu r}\right]^{1/3}. \tag{16}$$

3.1.5. Oil Film Velocity in Transverse Direction. From (3), the transverse component dF_θ of centrifugal force $d\mathbf{F}$ is

$$dF_\theta = -2\rho\omega v_r dV. \tag{17}$$

In much the same way as the derivation of that in radial direction, the oil film viscous shear stress $\tau_{z\theta}$ and relative velocity v_θ in the transverse direction could be deduced.

The elemental radial viscous shear stress $d\tau_{z\theta}$ acting on the control element two sides that are perpendicular to the z direction is

$$d\tau_{z\theta} = -\frac{dF_\theta}{dA} = \frac{2\rho\omega v_r dV}{dA} = 2\rho\omega v_r dz. \tag{18}$$

Substituting (13) into (18), we can obtain

$$\frac{d\tau_{z\theta}}{dz} = \frac{2\rho^2\omega^3 r}{\mu}\left[Hz - \frac{z^2}{2}\right]. \tag{19}$$

Equation (19) can be integrated to give

$$\tau_{z\theta} = \frac{2\rho^2\omega^3 r}{\mu}\left[\frac{Hz^2}{2} - \frac{z^3}{6} + C_3\right]. \tag{20}$$

At the free surface of the oil film, the transverse viscous shear stress $\tau_{z\theta} = 0$. Thus, the integration constant $C_3 = -H^3/3$. And then, at any internal position of the oil film, the transverse viscous shear stress $\tau_{z\theta}$ is given by

$$\tau_{z\theta} = \frac{\rho^2\omega^3 r}{3\mu}\left[2H^3 - 3Hz^2 + z^3\right]. \tag{21}$$

Similarly, with the constitutive equation for a Newtonian fluid, one obtains the relation between transverse viscous shear stress $\tau_{z\theta}$ and transverse velocity v_θ

$$\tau_{z\theta} = \mu\frac{\partial v_\theta}{\partial z}, \tag{22}$$

or

$$\frac{\partial v_\theta}{\partial z} = \frac{\rho^2\omega^3 r}{3\mu^2}\left[2H^3 - 3Hz^2 + z^3\right]. \tag{23}$$

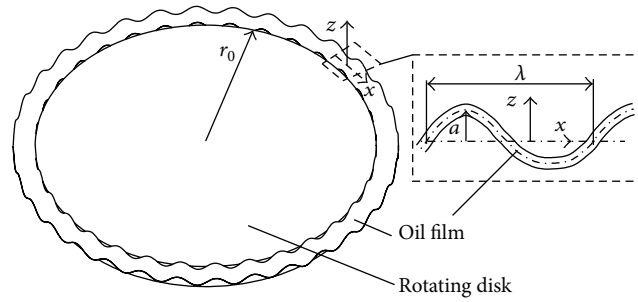

Figure 5: Schematic diagram of the oil film wave structure around rotating disk.

Equation (23) can be integrated to give

$$v_\theta = \frac{\rho^2\omega^3 r}{3\mu^2}\left[2H^3 z - Hz^3 + \frac{z^4}{4} + C_4\right]. \tag{24}$$

Obviously, the integration constant $C_4 = 0$. Furthermore, the oil film transverse velocity relative to rotating disk at any axial position z ($0 \le z \le H$) and the average relative transverse velocity, respectively, are

$$v_\theta = -\frac{\rho^2\omega^3 r}{12\mu^2}\left[8H^3 z - 4Hz^3 + z^4\right], \tag{25}$$

$$\overline{v_\theta} = \frac{\int_0^H v_\theta dz}{H} = -\omega r\left[\frac{3}{5}\left(\frac{2\rho Q^2}{3\pi^2\mu\omega r^4}\right)^{2/3}\right]. \tag{26}$$

The absolute transverse velocity of the oil film $\overline{v_t} = \omega r + \overline{v_\theta}$.

3.2. Oil Film Instability Near the Rotating Disk Edge. The oil film flowing on the rotating disk will become unstable due to the aerodynamic interaction between the oil film and its surrounding gas. The oil film instability is described by a wavelike motion. Generally speaking, the oil film wave amplitude is lower before spreading to the edge of the rotating disk. However, when the oil film flowing over or just off the edge, its velocity is very high and the wave amplitude will be increased strongly. Until the wave amplitude reaches a critical point, the film is disintegrated. At this point, the tears appear and the fragments of film whose lengths are equal to one wavelength are broken. Then, the surface tension forces these fragments to turn into lots of ligaments around the edge of rotating disk. Figure 5 illustrates the oil film wave structure around the edge of rotating disk schematically.

3.2.1. Wave Motion. In Figure 5, the wave motion equation of the oil film around the rotating disk is given by

$$z = a\sin\left(\frac{2\pi}{\lambda}x + \varepsilon\right), \tag{27}$$

where λ denotes the wave motion wavelength, ε denotes the phase angle, and a denotes the wave amplitude and it relates to the time

$$a = a_0\mathbf{e}^{\beta t}, \tag{28}$$

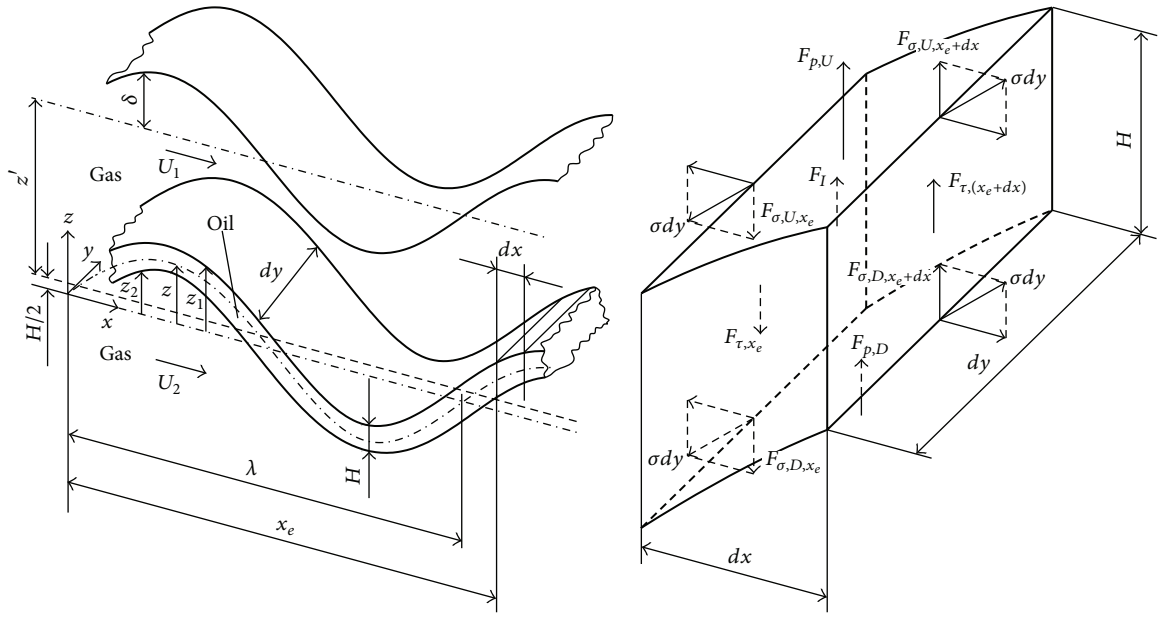

(a) Section of the wavy oil film

(b) Forces on the wavy oil film section

Figure 6: Section of the wavy oil film and the forces.

where a_0 denotes the initial wave amplitude, t denotes the time, and β denotes the growth rate of the wave amplitude.

3.2.2. Amplitude of Oil Film Wave Motion. Dombrowski et al. [21] deduced the forces which act on the liquid wave film moving through gas. As shown in Figure 6(a), the liquid film of thickness H moves in the x direction with the relative velocities of U_1 and U_2 at the upper and lower gas/liquid interfaces. The width of the film is dy in y direction. The film oscillated along z direction, when the film interface is flat; in other words, the film is undisturbed that is defined to be an equilibrium state. At the equilibrium state, it is defined that the x-axis coincides with the film midplane, and the axial coordinates of film upper and lower interfaces are $z_{\text{sta},U} = H/2$ and $z_{\text{sta},D} = -H/2$, respectively. When the film is disturbed, the deviation of film midplane from the x-axis is z, and the deviations of the upper and lower interfaces from the x-axis are z_1 and z_2, respectively. The deviations of the upper and lower interfaces from their equilibrium state are $z_1 - z_{\text{sta},U}$ and $z_2 - z_{\text{sta},D}$ respectively, that is, $z_1 - H/2$ and $z_2 + H/2$. It is known that $z_1 - H/2 = z_2 + H/2 = z$.

In addition, the gas surrounding the film will also be disturbed due to the interaction by wavy film. The displacement in z direction of the disturbed gas from its mean position δ is equal to the deviation of wavy film interface. The displacement of the disturbed gas near the upper and lower gas/liquid interfaces is all z.

3.2.3. Force Balance of Oil Film. At the position of $x = x_e$, we choose an infinitesimal oil film section of length dx which is shown in Figure 6(a) and it is enlarged in Figure 6(b). The sign convention is that the forces are positive if they point to the positive direction of the coordinate axe. The force analysis on the oil film section in z direction is carried out. The gas pressure forces on the oil film section top and bottom sides, where the z coordinates are z_1 and z_2, respectively, are given by $F_{p,U}$ and $F_{p,D}$. The viscous shear forces on the oil film section left and right sides, where the x coordinates are x_e and $x_e + dx$, respectively, are given by F_{τ,x_e} and $F_{\tau,(x_e+dx)}$. At the four arrises of oil film section which are parallel to the y direction, the surface tension forces are given by σdy and their directions are along the transverse direction of oil film surface. As shown in Figure 6(b), the components of the surface tension forces in z direction are F_{σ,U,x_e}, F_{σ,D,x_e}, F_{σ,U,x_e+dx}, and F_{σ,D,x_e+dx}. In addition to the above mentioned forces, the inertia force is given by F_I.

The calculation of the forces are as follows.

(1) Gas Pressure Force. For the oil film wave motion which is shown in Figure 6, Dombrowski et al. [21] proposed the pressure on the oil film surface p_U

$$p_U = k\rho_g U_1^2 \delta, \tag{29}$$

where ρ_g denotes the gas density and k denotes the wave number which is related to the wavelength λ by $k = 2\pi/\lambda$. The displacement of the disturbed gas in z direction δ is positive if it points to the positive direction of z coordinate axis. On the contrary, the displacement δ is negative. In this way, the gas pressure force on the top of oil film section is $F_{p,U} = kp_g U_1^2 z\, dy\, dx$. Similarly, the gas pressure force on the bottom of oil film section is $F_{p,D} = kp_g U_2^2 z\, dy\, dx$.

Thus, the resultant gas pressure force in z direction on the oil film section is

$$F_p = k\rho_g \left(U_1^2 + U_2^2\right) z\, dy\, dx, \tag{30}$$

where the velocities U_1 and U_2, which are mentioned in Section 3.2.2 and relate to the oil film and its surrounding gas velocities, are identified to be equal to each other and given by v. Therefore, the resultant gas pressure force on the oil film section F_p can be rewrote finally as

$$F_p = 2\rho_g k v^2 z\, dy\, dx. \tag{31}$$

(2) Surface Tension Force. We can easily verify that the components of the surface tension forces in z direction are $F_{\sigma,U,x_e} = \sigma\, dy(\partial z_1/\partial x)$ and $F_{\sigma,D,x_e} = \sigma\, dy(\partial z_2/\partial x)$. When the oil film upper and lower interfaces are parallel to each other, $\partial z_1/\partial x$ and $\partial z_2/\partial x$ are all equal to that of oil film midplane, namely, $\partial z/\partial x$. Therefore, at the two arrises of oil film section (where $x = x_e$), the superimposed surface tension force in z direction is

$$F_{\sigma,x_e} = \sigma\, dy\frac{\partial z_1}{\partial x} + \sigma\, dy\frac{\partial z_2}{\partial x} = 2\sigma\, dy\frac{\partial z}{\partial x}, \tag{32}$$

where σ denotes the fluid surface tension. Thus, in this case, at the other two arrises of oil film section (where $x = x_e + dx$), the superimposed surface tension force in z direction is

$$F_{\sigma,x_e+dx} = F_{\sigma,x_e} + \frac{\partial F_{\sigma,x_e}}{\partial x}dx. \tag{33}$$

After canceling out the term of F_{σ,x_e}, the resultant surface tension force in z direction on the oil film section F_σ can be rearranged finally as

$$F_\sigma = \frac{\partial}{\partial x}\left(2\sigma\, dy\frac{\partial z}{\partial x}\right)dx = 2\sigma\frac{\partial^2 z}{\partial x^2}dy\, dx. \tag{34}$$

(3) Inertia Force. It can be easily found that the mass of the oil film section is $\rho_l dy\, dx H$, and the velocity and acceleration are $\partial z/\partial t$ and $\partial^2 z/\partial t^2$, respectively. Thus, the inertia force on the oil film section F_I is

$$F_I = -\rho_1 H\frac{\partial^2 z}{\partial t^2}dy\, dx. \tag{35}$$

(4) Viscous Shear Force. For the oil film section which is shown in Figure 6(b), the viscous shear stress on the oil film section side (where $x = x_e$) is given by $\mu(\partial^2 z/\partial t\partial x)$. And then the viscous shear force on this side is easily found as follows:

$$F_{\tau,x_e} = \mu\frac{\partial^2 z}{\partial t\partial x}H\, dy, \tag{36}$$

where μ denotes the fluid dynamic viscosity. In this way, the viscous shear force on the other side (where $x = x_e + dx$) is

$$F_{\tau,x_e+dx} = F_{\tau,x_e} + \frac{\partial F_{\tau,x_e}}{\partial x}dx. \tag{37}$$

Lastly, the net viscous shear force on the oil film section F_τ is

$$\begin{aligned} F_\tau &= \frac{\partial}{\partial x}\left(\mu\, dyH\frac{\partial^2 z}{\partial t\partial x}\right)dx \\ &= \mu\left(\frac{H\partial^3 z}{\partial t\partial x^2} + \frac{\partial H}{\partial x}\frac{\partial^2 z}{\partial x\partial t}\right)dy\, dx. \end{aligned} \tag{38}$$

For the two interfaces of the oil film which are parallel to each other, $\partial H/\partial x = 0$. The second term on the right side of (38) could be canceled out. Then, the viscous shear force F_τ on the oil film section is changed to

$$F_\tau = \mu\frac{H\partial^3 z}{\partial t\partial x^2}dy\, dx. \tag{39}$$

3.2.4. Growth Rate of Disturbance. Equilibrium states of the oil film section in Figure 6(b) require that the sum of the gas pressure force F_p, the surface tension force F_σ, the inertia force F_I, and the viscous shear force F_τ is zero

$$F_p + F_\sigma + F_I + F_\tau = 0. \tag{40}$$

Substituting (31), (34), (35), and (39) into (40), we can obtain

$$2\rho_g k v^2 z + 2\sigma\frac{\partial^2 z}{\partial x^2} - \rho_l H\frac{\partial^2 z}{\partial t^2} + \mu H\frac{\partial^3 z}{\partial t\partial x^2} = 0. \tag{41}$$

For a sine wave, substituting the wave motion equation (27) into (41) gives

$$2\rho_g k v^2 a - 2\sigma k^2 a - \rho_l H\frac{\partial^2 a}{\partial t^2} - \mu H k^2\frac{\partial a}{\partial t} = 0, \tag{42}$$

and substituting (28) into (42) gives

$$2\rho_g k v^2 - 2\sigma k^2 - \rho_l H\frac{\partial^2(\beta t)}{\partial t^2} - \mu H k^2\frac{\partial(\beta t)}{\partial t} = 0, \tag{43}$$

or (43) is rearranged slightly and it is wrote as

$$2\rho_g k v^2 - 2\sigma k^2 - \rho_l H\beta^2 - \mu H k^2\beta = 0. \tag{44}$$

From (44), selecting the growth rate of the disturbance β as the unknown variable, the relation between β with the rest variables can be stated as follows:

$$\beta = \frac{-\mu H k^2 + \left[\mu^2 H^2 k^4 + 4\rho_l H\left(2\rho_g k v^2 - 2\sigma k^2\right)\right]^{1/2}}{2\rho_l H}, \tag{45}$$

where the oil film thickness H at the rotating disk edge could be obtained by replacing r with the rotating disk radius r_0 in (15). The relative velocity between the oil film and its surrounding gas v is calculated by the absolute value of oil film velocity v_0 minus its surrounding gas velocity v_g; namely, $v = |v_0 - v_g|$. The oil film velocity v_0 is the composition of radial and transverse velocities which are obtained by replacing r with the rotating disk radius r_0 in (16) and (26). The radial velocity could be neglected compared to the transverse velocity; that is, the oil film velocity v_0 is approximately the transverse velocity v_{0t}

$$v_0 = \sqrt{{v_{0r}}^2 + {v_{0t}}^2} \approx v_{0t}. \tag{46}$$

The transverse velocity v_{0t} is the absolute velocity; namely, the rotating disk edge linear velocity ωr_0 adds the average relative transverse velocity which is given by (26).

In recent years, many researchers have carried out the gas flow analysis in a bearing chamber [1, 22, 23], by means of the Laser Doppler Anemometry (LDA); the gas flow velocities were measured in bearing chambers under various operating conditions. For the sake of convenience and universality, in their work, the gas velocities were nondimensioned by the surface velocity of shaft; that is, $v_g^* = v_g/(\pi n_s r_0/30)$. v_g is the gas velocity and its dimension is m/s and n_s is the rotational speed of shaft. The experimental results indicated that the nondimensional gas velocities are relatively insensitive to the shaft rotational speed. Near the shaft surface, about 0.5 mm, the nondimensional gas velocity is about 0.8 [1, 23]. Then, in the present work, the gas flow regime near the oil film which has a negligible relative velocity to rotating disk is similar to the situation of bearing chamber shaft. Therefore, the gas velocity near the oil film is reasonably treated as

$$v_g = 0.8 * \left(\frac{\pi n_s r_0}{30}\right). \tag{47}$$

3.3. Ligament Number and Droplet SMD. The wave film will disintegrate at its most unstable state and the fragments which are caused by disintegration rapidly contract into lots of ligaments under the action of surface tension. Based on the classical Rayleigh-Weber theory, the disturbance with maximum growth rate $\beta_{\max}$ would lead to the disintegration of the film. To apply the method which is mentioned in Section 3.1 about the oil film flow analysis under specific geometry and operating conditions, the oil film thickness and velocity at the rotating disk edge, as well as the oil and gas properties, are particular. In this way, the growth rate β in (45) only relates to one variable that is the wave number k. Therefore, the maximum growth rate $\beta_{\max}$ could be calculated by

$$\frac{d\beta}{dk} = 0. \tag{48}$$

Equations (45) and (48) could be solved simultaneously. The wave number corresponding to the maximum growth rate $\beta_{\max}$ is obtained and here wrote as k_{dis}. In addition, the wavelength of oil film disintegration $\lambda_{\text{dis}} = 2\pi/k_{\text{dis}}$. Therefore, the number of total ligaments around rotating disk edge N is given by

$$N = \frac{2\pi r_0}{\lambda_{\text{dis}}}. \tag{49}$$

The ligament diameter d_L and droplet SMD d_{32} are [24]

$$\begin{aligned} d_L &= 2\left(\frac{Hr_0}{N}\right)^{0.5}, \\ d_{32} &= \left[\frac{3}{2}\sqrt{2}\pi {d_L}^3 \left(1 + 3Oh_L\right)^{0.5}\right]^{1/3}, \end{aligned} \tag{50}$$

where the Ohnesorge number $Oh_L = \mu/(\rho_l \sigma d_L)^{0.5}$.

4. Results and Discussion

The geometry and operating parameters which are adopted in the theoretical analysis are shown in Table 1. Unless otherwise specified, the variables values are fixed on the middle of the last column.

Table 1: Geometry and operating parameters.

Rotating disk radius r_0 (mm)	45	60	75
Rotational speed n_s (r/min)	4000	6000	8000
Oil volume flow rate Q (L/h)	75	150	225
Oil density ρ (kg/m^3)	903.5	953.5	1003.5
Oil dynamic viscosity μ (Pa·s)	0.0351	0.0276	0.0201

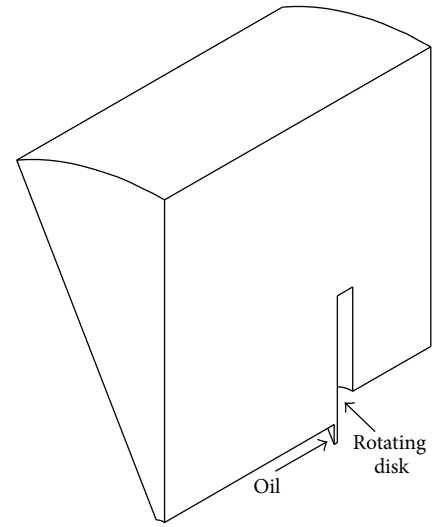

Figure 7: Computational domain of oil film on a rotating disk.

4.1. Validity of the Assumptions. To illustrate the validity of the assumptions which are mentioned in Section 3.1.2, a comprehensive approach based on the Computational Fluid Dynamics (CFD) is adopted. The equations of continuity and motion for the liquid flow on a rotating disk were listed by Higgins [25]. Some analyses on the liquid flow on a rotating disk were carried out by a numerical simulation. The description of the numerical approach is not included here and the interested reader is referred to the literatures, for example, [26, 27]. Here, we resort to the same approach. The computational domain of oil film on a rotating disk is shown in Figure 7. The oil film flowing on the rotating disk is axisymmetric; thus, the domain whose range is 30° in transverse direction is chosen as the calculation domain. And the domain is discretized with the structured grid which only contains a lot of hexahedral cells. The pressure boundary condition is that the relative pressure of the outlet is zero. The mass boundary condition on the oil inlet is the mass flow rate which is equal to the oil flow. The enclosed walls are stationary or rotating (the surface of rotating disk) with no-slip conditions applied.

The oil film flowing on the rotating disk is calculated using the commercial CFD package CFX. Under the conditions of $r_0 = 75$ mm, $Q = 150$ L/h, and three different rotational speeds, the comparison of data by (26) and data by CFD is shown in Figure 8. It is found that (26) which is proposed in

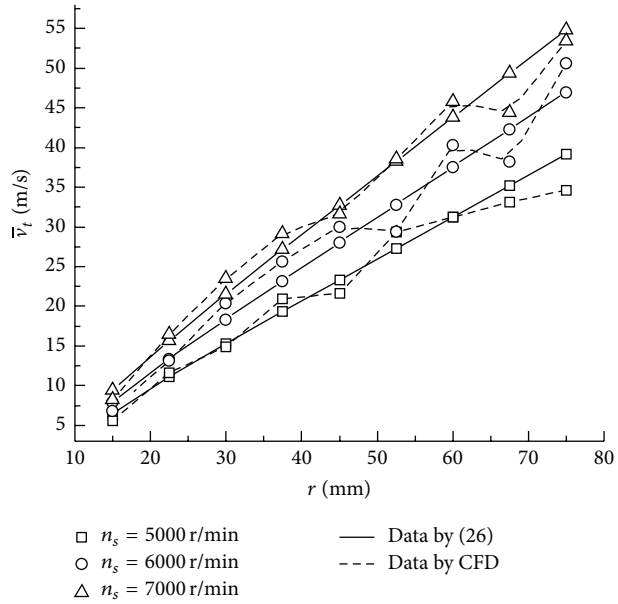

Figure 8: Comparison of data by (26) and data by CFD.

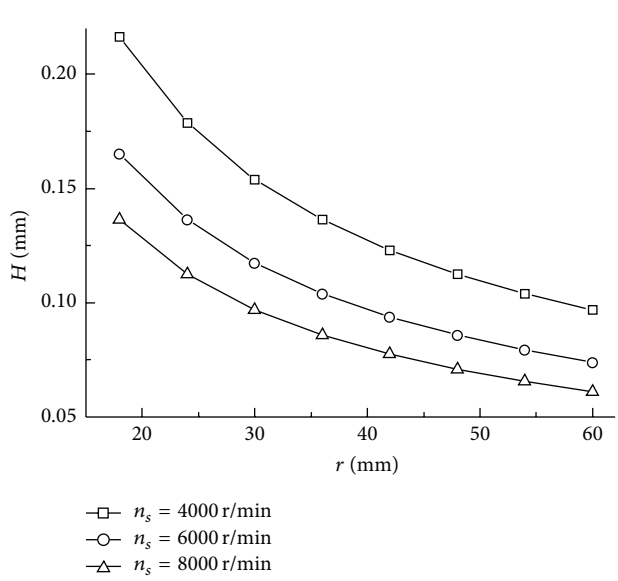

Figure 9: Influence of rotational speed on oil film thickness.

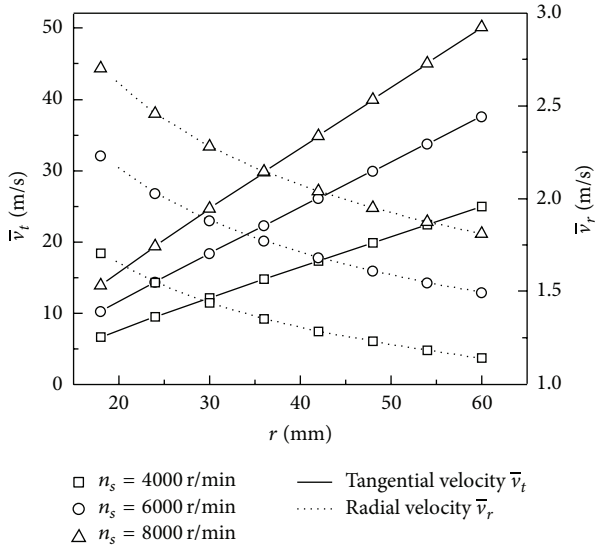

Figure 10: Influence of rotational speed on oil film average velocities.

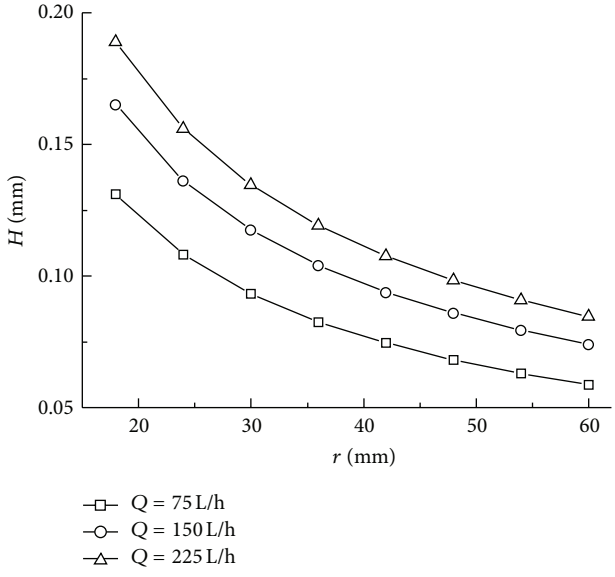

Figure 11: Influence of oil volume flow rate on oil film thickness.

the present work could evaluate the oil film flow on a rotating disk with a relative small discrepancy to the CFD approach that is about 15%. It is concluded that the analysis model, which is proposed in Section 3.1, is therefore an acceptable simplification.

4.2. Oil Film Velocity and Thickness. Figure 9 summarizes the influence of rotating disk rotational speed on oil film thickness. It can be found that, keeping away from the rotating disk rotational axis, the oil film thickness is decreased gradually. That attributes to, under a constant volume flow rate, with the oil film spreading on rotating disk, the fact that the sectional area of the oil film along transverse direction is increased. As a consequence, the oil film becomes thinner. In addition, the oil film thickness is decreased with the increasing rotational speed. The reason is that the centrifugal force is increased with increasing rotational speed. That leads to the fact that the oil film radial velocity is increased, and, in return, the oil film also becomes thinner.

Figure 10 summarizes the influence of rotating disk rotational speed on oil film average velocities. As mentioned earlier, the higher rotational speed enlarges the centrifugal force, as well as the oil film average radial velocity. It is easily understood that with increasing rotational speed the transverse velocity of rotating disk is increased.

Figures 11 and 12 suggest the effect of oil volume flow rate on oil film thickness and average velocities. Apparently, the oil film thickness will be increased with increasing oil volume

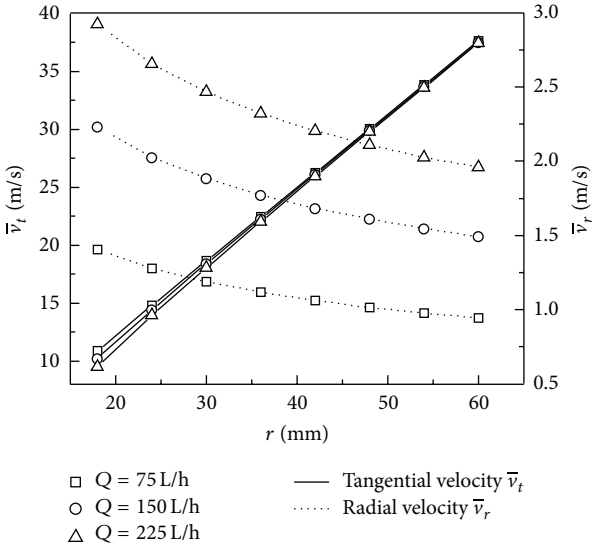

Figure 12: Influence of oil volume flow rate on oil film velocity.

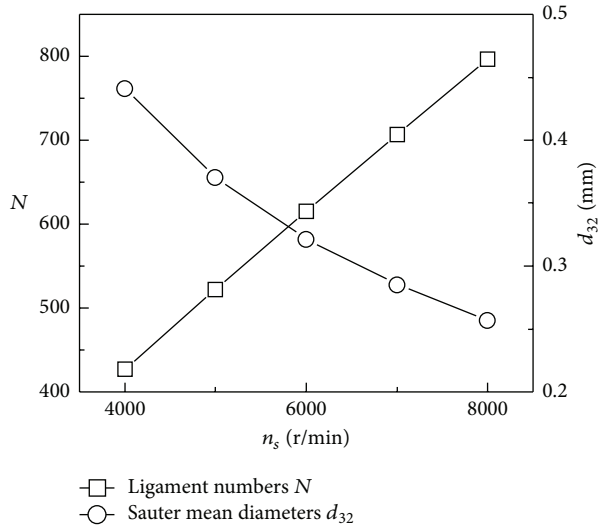

Figure 13: Variation in ligament number and droplet SMD with rotational speed.

flow rate. Moreover, the oil film average transverse velocity is slightly decreased with increasing oil volume flow rate near the rotational axis. The reason is that the oil is accumulated near this position and it is hardly driven by the rotating disk, so the transverse velocity is decreased. However, when far from rotational axis, the oil flowing in radial direction has enough time to be driven by the rotating disk, so the effect of oil volume flow rates on transverse velocity becomes weak. Differently, the oil film average radial velocity is increased with increasing oil volume flow rate. The reason for that is when the oil film thickness is increased, the constraint of rotating disk in radial direction becomes weak and so the oil film easily flows in this direction; as a result, the radial velocity is increased.

4.3. Ligament Number and Droplet SMD. Figures 13 and 14 suggest the effect of rotating disk rotational speed and radius on ligament number and droplet SMD. It is observed that the ligament numbers are all increased with increasing rotating disk radius and rotational speed. That is because the oil film flowing on the rotating disk will obtain more energy with increasing rotating disk radius and rotational speed, and, as a result, the disintegration of oil film is more considerable and ligament numbers are increased. As a result, the ligament diameters are decreased, and the droplet SMD will be decreased.

Figure 15 suggests the variation in ligament number and droplet SMD with the oil flow rate. It is observed that the ligament number is decreased with increasing oil flow rate. This is likely because the increasing oil flow rate leads the unit mass oil film to obtain less energy from the rotating disk, and, on the whole, the oil film disintegration becomes nonsignificant and the ligament number is decreased. As a consequence, the droplet SMD will be increased with the increasing ligament diameter.

As shown in Figure 16(a), the oil density has a less significant effect on the ligament number that is because

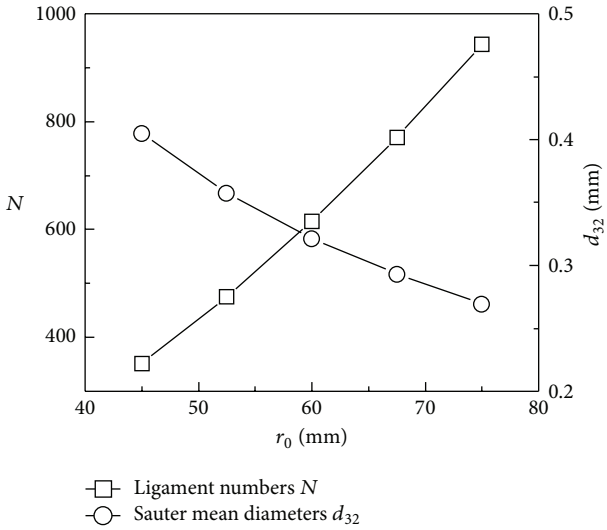

Figure 14: Variation in ligament number and droplet SMD with rotating disk radius.

the increasing oil density is expected to have little effect on the oil film thickness and velocity. And so the oil film wave strength does not change consequently. Furthermore, the ligaments nearly maintain a constant number. The droplets SMD also nearly remains unchanged. However, as shown in Figure 16(b), the oil viscosity has a significant effect on the ligament number, in detail, and the ligament number is decreased with an increasing oil viscosity that is because the increasing oil viscosity leads to an increasing oil film thickness and transverse velocity, and the oil film wavy characteristic becomes weak. In addition, the droplets SMD is increased.

5. Experimental Study

5.1. Test Facility. The test facility structure of rotating disk ligament number analysis is shown in Figure 17(a). A rotational

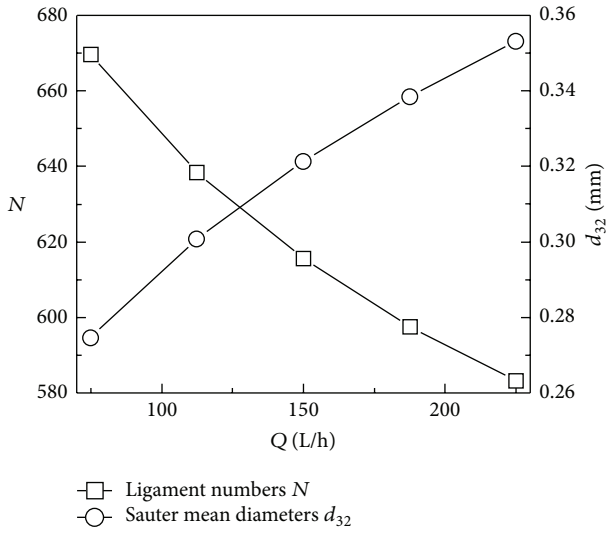

Figure 15: Variation in ligament number and droplet SMD with oil flow rate.

disk, which is an abstraction of the oil droplet generation sources in bearing chamber, is fixed on the end of a shaft by a cylinder pin in a cantilever arrangement. The shaft, which is positioned by two bearings, is driven by a variable frequency motor with a diaphragm coupling. The rotational speed of shaft is adjusted using an inverter. The oil is pumped from oil reservoir and orderly flows through components of lubrication system which mainly consists of relief valve, pressure reducing valve, volumetric flow meter, flow control valve, and so forth. The oil is fed along centerline onto the rotational disk using an injection pipe. And then the oil film is spread on the disk flush surface. The oil film is disintegrated at the disk edge and changes to a lot of ligaments. Lastly, the oil is collected at the housing walls. Gravitation forces the oil to flow back to the oil reservoir. The oil heater which is linked to a temperature controller is inserted into the oil reservoir, and the oil is maintained at a required temperature. The rotating disk chamber is bounded by the thin-walled transparent Perspex hollow cylinder and cover to ensure a visualization and enough illumination. The rotating disk chamber cover has a fan-shaped window which allows the high speed camera to collect the ligament image. The physical map of the test facility is shown in Figure 17(b).

5.2. Key Geometry and Performance Parameters of Test Facility. The rotational disk diameter is 150 mm. The stationary housing inner diameter and width are 350 and 159 mm. The high speed camera is Phantom v4.3 which is produced by Vision Research Company, and the detailed information about the camera is shown in [28]. As shown in Table 2, the L-HM 32 hydraulic oil is used in the experiment and it has similar properties to the oil which is applied to an aeroengine bearing chamber, for example, Mobil Jet 2.

5.3. Measuring Techniques of Oil Ligament Number. The experimental objectives of this paper, namely, the quantitative characterization of ligament, required applying technique for ligament visualization. In this paper, the high speed camera is used to obtain a detailed documentation of the oil ligament around the rotating disk edge. The high speed camera is linked to a computer and the oil ligaments are monitored on a screen. And then it is recorded on a hard disk and examined in detail using picture processing software Cine Viewer Application which is attached to the high speed camera. As shown in Figure 18, an angle scales disk, whose resolution is 1°, is fixed near the rotational disk edge. The high speed camera can clearly record the oil ligaments and the scale simultaneously. The total number of the oil ligaments around the whole edge of rotating disk can be computed with the ligaments covering the scale. As shown in Figure 18, an angle range $\theta = 381.7 - 349.6 = 32.1^\circ$, and it has 11 ligaments in the angle range; the total number of the ligaments around the whole edge of rotating disk $N = 11 * 360/32.1 \approx 123$. The ligament number under other conditions could also be obtained with this method.

Table 2: Properties comparison of L-HM 32 hydraulic oil and Mobil Jet 2 lubricant oil.

	L-HM 32	Mobil Jet 2
Kinematic viscosity (mm^2/s)		
40°C	30.69	27.6
100°C	5.28	5.1
Density (kg/m^3)	874.8	1003.5

5.4. Comparison of Theoretical and Experimental Data. Under the operating parameters, rotating disk radius $r_0 = 75$ mm, oil density $\rho_l = 866\,kg/m^3$, oil dynamic viscosity $\mu = 0.02658$ Pa·s, surface tension $\sigma = 0.036$ N/m, and gas density $\rho_g = 1.165\,kg/m^3$, the ligament numbers are obtained at different rotational speeds and oil flow rates by theoretical and experimental methods, respectively. Figure 19 shows the comparison between the theoretical and experimental data. It is clear that the values of ligament number which is predicted from the present paper theoretical method fit quite well the experimental data.

It is a pity that, because the test facility vibrates obviously at high shaft speed, the shaft speeds of experimental analysis are lower than those of bearing chamber. As a supplement, with the help of others' experimental data [5–7], the comparison between theoretical and experimental droplet SMD at high shaft speed is shown in Table 3. The oil which is used in the experiment was Mobil Jet 2, and the shaft speed ranged between 3450 and 8500 r/min. It is demonstrated that the theoretical method could predict the oil droplet SMD with relative small deviations. Therefore, the theoretical model which is proposed in the present paper is valid for investigation of oil droplet generation process on a rotating disk.

6. Conclusions

The present investigation focused on the characterization of oil film on a rotating disk, as well as ligament number and

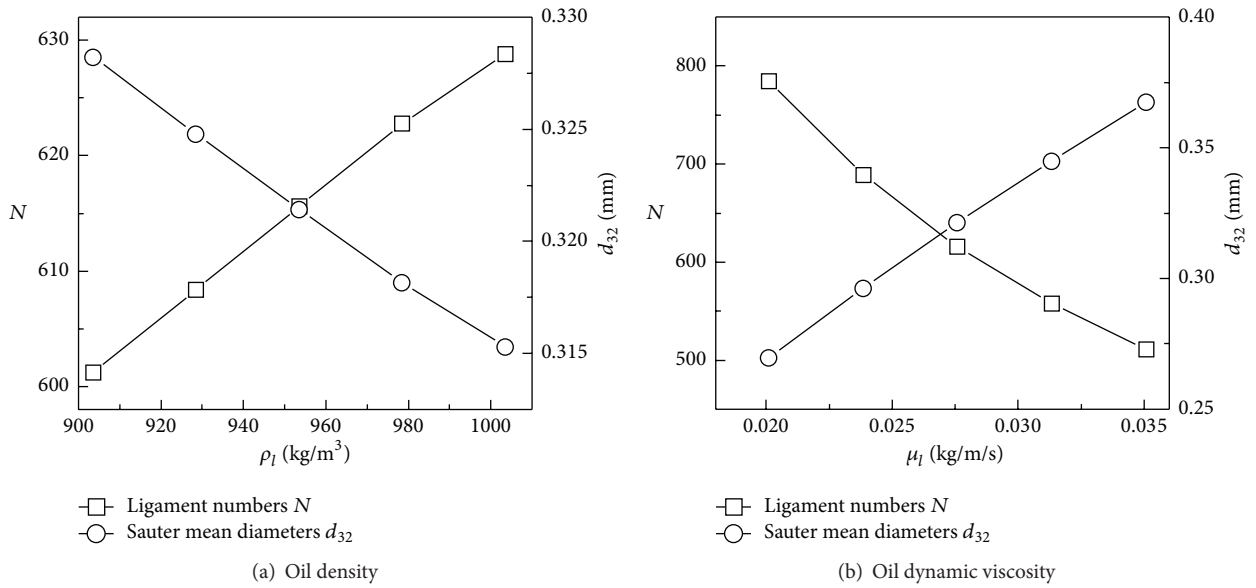

(a) Oil density (b) Oil dynamic viscosity

Figure 16: Variation in ligaments number and droplets SMD with oil properties.

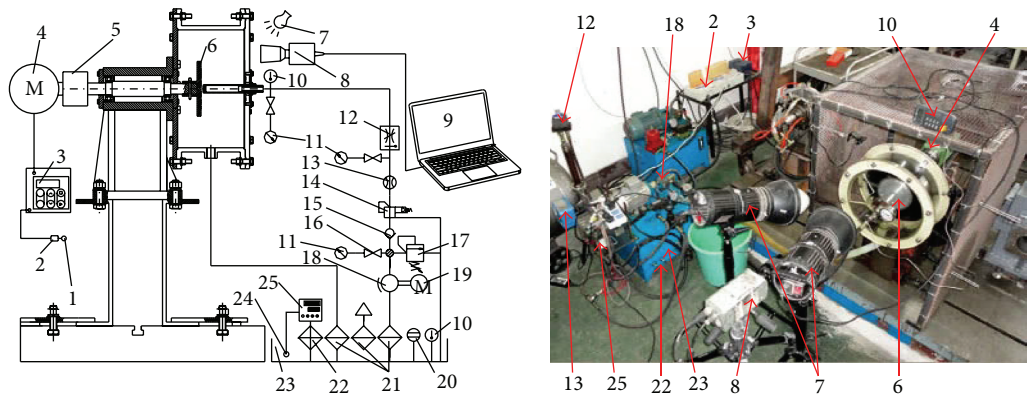

(a) Structure diagram (b) Physical map

Figure 17: Rotating disk ligament number analysis test facility. 1: power; 2: air circuit breaker; 3: inverter; 4: variable frequency motor; 5: diaphragm coupling; 6: rotational disk; 7: photography lights; 8: high speed camera; 9: computer; 10: thermometer; 11: pressure gage 12: flow control valve; 13: volumetric flow meter; 14: pressure reducing valve; 15: check valve; 16: stop valve; 17: relief valve; 18: oil pump; 19: motor; 20: level gauge; 21: filter; 22: oil heater; 23: oil reservoir; 24: thermocouple; 25: temperature controller.

Table 3: Comparison of theoretical and experimental oil droplet SMD.

r_0 (mm)	n_s (r/min)	Q (L/h)	d_{32} (μm)	
			Experimental data [5–7]	Theoretical data
100	5000	103	212.0	201.2
55	8500	60	121.2	109.8
65	3450	50	228.4	212.1

droplet SMD, which are generated by integration of oil film. From the calculation, it is observed that

(1) with increasing rotational speeds, the oil film thickness is decreased, while the radial and transverse velocities are increased; the rotating disk radius has no effect on the oil film thickness and velocity; with increasing oil flow rates, the thickness and radial velocity are increased, but the transverse velocity is decreased;

(2) with increasing disk rotational speeds and radiuses, the ligament numbers are increased, while with the increasing oil flow rates and viscosities the ligaments numbers are decreased; the oil density has less effect on the ligament number;

(3) with increasing rotational speeds, disk radiuses, and oil densities, the oil droplet SMD is decreased, while with increasing oil flow rates and viscosities the ligaments numbers are increased.

A test facility is also built, and the ligament numbers are measured under different conditions. The comparisons

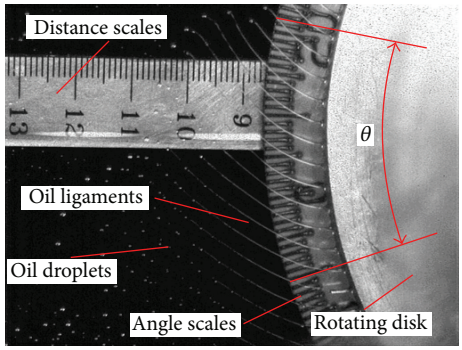

Figure 18: Measuring techniques of oil ligaments.

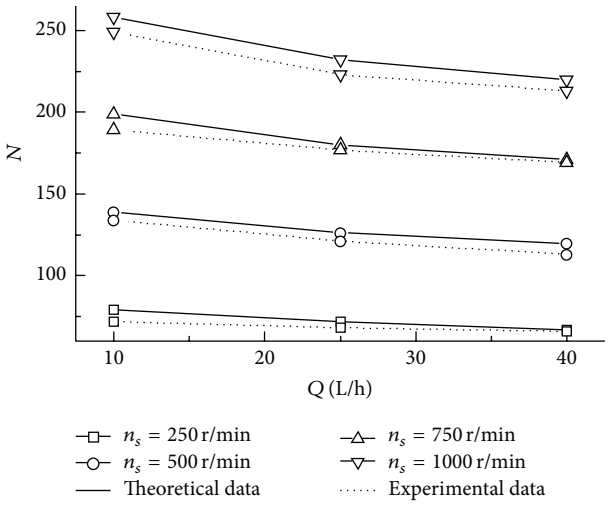

Figure 19: Comparison of theoretical and experimental ligament.

between theoretical and experimental ligament number, as well as oil droplet SMD, show that the theoretical method is reliable. The work of the present paper may contribute to understanding the oil droplet generation in a bearing chamber. However, the oil droplet generation in bearing chamber was strongly affected by more factors. Additional and more advanced approaches are necessary to further improve the theoretical model.

Conflict of Interests

The authors declare that there is no conflict of interests regarding the publication of this paper.

Acknowledgment

The authors gratefully acknowledge the financial support of the National Natural Science Foundation of China (Grant no. 51275411).

References

[1] A. Glahn, M. Kurreck, M. Willmann, and S. Wittig, "Feasibility study on oil droplet flow investigations inside aero engine bearing chambers—PDPA techniques in combination with numerical approaches," *Journal of Engineering for Gas Turbines and Power*, vol. 118, no. 4, pp. 749–755, 1996.

[2] P. Gorse, K. Dullenkopf, H.-J. Bauer, and S. Wittig, "An experimental study on droplet generation in bearing chambers caused by roller bearings," in *Proceedings of ASME Turbo Expo: Power for Land, Sea and Air*, pp. 1681–1692, Berlin, Germany, June 2008.

[3] M. Shimo, J. V. Canino, and S. D. Heister, "Modeling oil flows on seal runners and engine sump walls," *ASME Journal of Engineering for Gas Turbines and Power*, vol. 127, no. 4, pp. 827–834, 2005.

[4] M. P. Krug, P. Davide, K. Wolfram et al., "Experimental investigation into the efficiency of an aero engine oil jet supply system," in *Proceedings of the ASME Turbo Expo: Turbine Technical Conference and Exposition*, Dusseldorf, Germany, June 2014.

[5] A. Glahn, S. Busam, M. F. Blair, K. L. Allard, and S. Wittig, "Droplet generation by disintegration of oil films at the rim of a rotating disk," *Journal of Engineering for Gas Turbines and Power*, vol. 124, no. 1, pp. 117–124, 2002.

[6] A. Glahn, M. F. Blair, K. L. Allard, S. Busam, O. Schäfer, and S. Wittig, "Disintegration of oil jets emerging from axial passages at the face of a rotating cylinder," *Journal of Engineering for Gas Turbines and Power*, vol. 125, no. 4, pp. 1003–1010, 2003.

[7] A. Glahn, M. F. Blair, K. L. Allard, S. Busam, O. Schäfer, and S. Wittig, "Disintegration of oil films emerging from radial holes in a rotating cylinder," *Journal of Engineering for Gas Turbines and Power*, vol. 125, no. 4, pp. 1011–1020, 2003.

[8] K. Simmons, S. Hibberd, Y. Wang, and I. Care, "Numerical study of the two-phase air/oil flow within an aero-engine bearing chamber model using a coupled Lagrangian droplet tracking method," in *Proceedings of the ASME Prssure Vessels and Piping Conference*, pp. 325–331, Vancouver, Canada, August 2002.

[9] M. Farrall, S. Hibberd, and K. Simmons, "The effect of initial injection conditions on the oil droplet motion in a simplified bearing chamber," *ASME Journal of Engineering for Gas Turbines and Power*, vol. 130, no. 1, Article ID 012501, 2008.

[10] B. Chen, G. D. Chen, H. C. Sun, and Y. H. Zhang, "Effect of oil droplet deformation on its deposited characteristics in an aeroengine bearing chamber," *Proceedings of the Institution of Mechanical Engineers G: Journal of Aerospace Engineering*, vol. 228, no. 2, pp. 206–218, 2014.

[11] A. Glahn and S. Wittig, "Two-phase air/oil flow in aero engine bearing chambers: characterization of oil film flows," *Journal of Engineering for Gas Turbines and Power*, vol. 118, no. 3, pp. 578–583, 1996.

[12] Y.-Y. Wang, S.-F. Wang, J.-F. Ai, and B. Li, "Experimental verification of numerical simulation of oil-air two-phase flow in bearing chamber," *Journal of Aerospace Power*, vol. 28, no. 3, pp. 629–635, 2013.

[13] G. D. Chen, H. C. Sun, and J. Wang, "Research into configuration and flow of wall oil film in bearing chamber based on droplet size distribution," *Chinese Journal of Aeronautics*, vol. 24, no. 3, pp. 355–362, 2011.

[14] Z. X. Liu, J. Y. Zhao, J. P. Hu, and Y. G. Lu, "A numerical model for unsteady oil film motion in aero-engine bearing chambers and experimental verification," in *Proceedings of the Gas Turbine India Conference (GTINDIA '13)*, ASME, Bangalore, India, December 2013.

[15] S. Wittig, A. Glahn, and J. Himmelsbach, "Influence of high rotational speeds on heat transfer and oil film thickness in aero-engine bearing chambers," *Journal of Engineering for Gas Turbines and Power*, vol. 116, no. 2, pp. 395–401, 1994.

[16] A. R. Frost, "Rotary atomization in the ligament formation mode," *Journal of Agricultural Engineering Research*, vol. 26, no. 1, pp. 63–78, 1981.

[17] Y. Y. Zhao, "Analysis of flow development in centrifugal atomization: part I. Film thickness of a fully spreading melt," *Modelling and Simulation in Materials Science and Engineering*, vol. 12, no. 5, pp. 959–971, 2004.

[18] Y. Y. Zhao, "Analysis of flow development in centrifugal atomization: part II. Disintegration of a non-fully spreading melt," *Modelling and Simulation in Materials Science and Engineering*, vol. 12, no. 5, pp. 973–983, 2004.

[19] J. X. Liu, Q. B. Yu, and Q. Qin, "Numerical study on film disintegration by centrifugal atomisation using rotating cup," *Powder Metallurgy*, vol. 56, no. 4, pp. 288–294, 2013.

[20] M. W. Frank, *Fluid Mechanics*, McGraw-Hill, Boston, Mass, USA, 4th edition, 1998.

[21] N. Dombrowski and W. R. Johns, "The aerodynamic instability and disintegration of viscous liquid sheets," *Chemical Engineering Science*, vol. 18, no. 3, pp. 203–214, 1963.

[22] P. Gorse, K. Willenborg, S. Busam et al., "3D-LDA measurements in an aero-engine bearing chamber," in *Proceedings of the ASME Turbo Expo: Power for Land, Sea and Air*, pp. 257–265, Atlanta, Ga, USA, June 2003.

[23] P. Gorse, S. Busam, and K. Dullenkopf, "Influence of operating condition and geometry on the oil film thickness in aeroengine bearing chambers," *Journal of Engineering for Gas Turbines and Power*, vol. 128, no. 1, pp. 103–110, 2006.

[24] N. Ashgriz, *Handbook of Atomization and Sprays*, Springer, London, UK, 2011.

[25] B. G. Higgins, "Film flow on a rotating disk," *Physics of Fluids*, vol. 29, no. 11, pp. 3522–3529, 1986.

[26] I. Leshev and G. Peev, "Film flow on a horizontal rotating disk," *Chemical Engineering and Processing: Process Intensification*, vol. 42, no. 11, pp. 925–929, 2003.

[27] Y. Y. Zhao, M. H. Jacobs, and A. L. Dowson, "Liquid flow on a rotating disk prior to centrifugal atomization and spray deposition," *Metallurgical and Materials Transactions B: Process Metallurgy and Materials Processing Science*, vol. 29, no. 6, pp. 1357–1369, 1998.

[28] http://www.visionresearch.com/.